

NUMERICAL INVESTIGATIONS ON SOLUTE TRANSPORT AND FRECKLE FORMATION DURING DIRECTIONAL SOLIDIFICATION OF NICKLE-BASED SUPERALLOY INGOT

by

**Jiajun CUI^{a,b}, Baokuan LI^{a*}, Zhongqiu LIU^a,
Fengsheng QI^a, and Beijiang ZHANG^b**

^a School of Metallurgy, Northeastern University, Shenyang, China

^b High Temperature Materials Research Division, Central Iron and Steel Research Institute,
Beijing, China

Original scientific paper

<https://doi.org/10.2298/TSCI210826339C>

In order to investigate the solute distribution and freckles formation during directional solidification of superalloy ingots, a mathematical model with coupled solution of flow field, solute and temperature distribution was developed. Meanwhile, the reliability of this model was verified by the experimental and simulation results in relevant literatures. The 3-D directional solidification process of Ni-5.8 wt.% Al-15.2 wt.% Ta superalloy ingot was simulated, and then the dynamic growth of solute enrichment channels was demonstrated inside the ingot. Freckles formation under different cooling rates was studied, and the local segregation degree inside the ingot was obtained innovatively after solidification. The results show that the number of freckles formed at the top gradually decreases, and so do the degree of solute enrichment at these freckles with the increase of cooling rate. Moreover, the relative and volume-averaged segregation ratio is defined to describe the segregation degree inside the ingot. The span of relative segregation ratio for positive segregation is wider than that for negative segregation, but it accounts for less of total volume. As the cooling rate increases from 0.1 K/s to 1.0 K/s, the proportion of weak segregation (-20%~20%) increases significantly from 26% to 41%, so that the segregation degree is weakened in general. By analyzing the freckles formation and segregation degree inside the ingot, the numerical simulation results can provide a theoretical basis for optimizing the actual production process to suppress the freckle defects.

Key words: nickel-based superalloy, directional solidification,
channel segregation, freckle formation, numerical simulation

Introduction

Directional solidification technology can control the grain orientation so that all grain boundaries are parallel to the height direction of the casting. The casting produced by this technology has longer fatigue life and higher creep resistance, thus becoming the main process in the production of alloy components for advanced manufacturing industries, such as aerospace, automobile and medical care [1]. However, the change of liquid density caused by thermal and solute concentration gradient usually cause the thermosolutal convection, which may lead to elongated solute enrichment channels [2]. These channels usually can not be

* Corresponding author, e-mail: libk@smm.neu.edu.cn

eliminated by heat treatment or rolling process after solidification, showing as spot defects, also known as freckles [3]. Nickel-based superalloy castings, which are mainly used in the manufacture of key hot-end components of aero-engines and large gas turbines, are more prone to such defects [4]. This has led to a great increase in the scrap rate, thus increasing the production cost and energy consumption.

In order to optimize the directional solidification process and reduce the formation of freckles, it is very significant to understand the formation mechanism of freckles and clarify the basic relationship between the freckles and the main process parameters. Scholars have conducted extensive and in-depth research by experiments and numerical simulation. Wang *et al.* [5] observed the macro-segregation phenomenon in the vertical directional solidification process of Pb-15 wt.% Sn and Sn-15 wt.% Pb alloys, and found that obvious freckles extending to the upper half of the steel ingot appeared in the lead-rich alloy, while no obvious macro-segregation phenomenon appeared in the tin-rich alloy under the same conditions. Shevchenko *et al.* [6, 7] developed an in-situ radiography technology to investigate the formation of stable channels under several solidification conditions. It was found that the dendrite fragments caused by remelting tended to stay in the channels, proving that channel segregation is necessary for the formation of freckles. Felicelli [8] predicted the thermosolutal convection and channel segregation during directional solidification of multi-component alloys based on the continuum model established by Bennon and Incropera [9]. Guo and Beckermann [10] and Sung *et al.* [11], respectively, reported the effect of grid spacing on the simulation results of freckle formation in lead-tin alloy and nickel-based superalloy, and also proposed a more reasonable grid spacing in the numerical calculation. Sun *et al.* [12] simulated the formation of freckles during directional solidification of nickel-based superalloy castings under the condition of cross-section shrinkage. The results show that cross-section shrinkage leads to the increase of local permeability in the mushy zone, which promotes the formation of freckles. Kumar *et al.* [13] considered the effect of different permeability laws in the mushy zone on the prediction of macro-segregation and channel segregation, and found that the prediction results of channel segregation are more easily affected by permeability changes than the former.

However, most of the simulation studies on 3-D directional solidification only predict the formation of freckles at the overall level, and fail to fully demonstrate the growth phenomenon of solute enrichment channels until now. Meanwhile, to the best of our knowledge, there are few literatures that predict the local degree of segregation inside the ingot after solidification. In this work, the channel segregation and freckle formation are reproduced at the global level, and the dynamic growth phenomenon of solute enrichment channels in the ingot is shown during directional solidification of Ni-5.8 wt.% Al-15.2 wt.% Ta superalloy ingot. Subsequently, the effect of cooling rate on freckle formation was analyzed and discussed. In particular, the local degree of segregation was innovatively obtained from a local point of view inside the ingot after solidification.

Mathematical model

Governing equations

Taking into account heat transfer, solute transport, and buoyancy driven flow during directional solidification of a multicomponent alloy, the prediction model for freckles is developed in this paper. The following assumptions are used in the model: the Boussinesq approximation is employed to consider the laminar flow driven by thermosolutal buoyancy, the

solidification process satisfies the local thermodynamic equilibrium and the solid phase is assumed to be motionless, and the mushy zone is approximately an isotropic porous medium and its permeability model is described by the Carman-Kozeny relation. On the basis of the above simplifications, the full details of the prediction model are presented [14-17]:

Mass conservation:

$$\nabla \vec{V} = 0 \quad (1)$$

Momentum conservation:

$$\frac{\partial}{\partial t}(\rho u) + \nabla(\rho \vec{V}u) = \nabla(\mu \nabla u) - \frac{\partial p}{\partial x} - \frac{\mu}{K}u \quad (2)$$

$$\frac{\partial}{\partial t}(\rho v) + \nabla(\rho \vec{V}v) = \nabla(\mu \nabla v) - \frac{\partial p}{\partial y} - \frac{\mu}{K}v \quad (3)$$

$$\frac{\partial}{\partial t}(\rho w) + \nabla(\rho \vec{V}w) = \nabla(\mu \nabla w) - \frac{\partial p}{\partial z} - \frac{\mu}{K}w + S_g \quad (4)$$

where S_g indicates the effect of density difference caused by the gradient of temperature and solute concentration of mushy zone on the flow. It can be derived explicitly from:

$$S_g = \rho g [\beta_T(T - T_{ref}) + \sum_i \beta_C(C_1^i - C_{1,ref}^i)] \quad (5)$$

As dendrite gap in mushy zone is assumed to be treated as porous medium, the permeability of Darcy resistance term without regard to solidification shrinkage can be described:

$$K = \frac{\delta^2}{180} \frac{f_1^3}{(1 - f_1)^2} \quad (6)$$

The liquid fraction f_1 can be obtained from the following expression:

$$f_1 = \begin{cases} 0 & T \leq T_{sol} \\ \frac{T - T_{sol}}{T_{liq} - T_{sol}} & T_{sol} < T \leq T_{liq} \\ 1 & T > T_{liq} \end{cases} \quad (7)$$

Energy conservation:

$$\frac{\partial}{\partial t}(\rho h) + \nabla(\rho \vec{V}h) = \nabla \left(\frac{\lambda}{c_p} \nabla h \right) + \nabla \left[\frac{\lambda}{c_p} \nabla (h_s - h) \right] - \nabla[\rho \vec{V}(h_1 - h)] \quad (8)$$

where $h = c_p T + f_1 L$, $h_1 = c_p T_{liq} + L$, and $h_s = c_p T_{sol}$.

Solute conservation:

$$\frac{\partial}{\partial t}(\rho C^i) + \nabla(\rho \vec{V}C^i) = \nabla(\rho D \nabla C^i) + \nabla[\rho D \nabla(C_1^i - C^i)] - \nabla[\rho(C_1^i - C^i)\vec{V}] \quad (9)$$

where $C^i = f_1 C_1^i + f_s C_s^i$, $C_s^i = k_p C_1^i$, and $f_1 + f_s = 1$.

According to these equations, the solid fraction f_s can be obtained by:

$$f_s = \frac{1}{1 - k_p} \frac{T - T_{\text{liq}}}{T - T_m} \quad (10)$$

In order to close the governing equations of fluid-flow, heat transfer and solute transport aforementioned and realize their coupling solution, it is necessary to supplement the relationship between liquid fraction and solute concentration. The phase diagram method is used to update the solid fraction during solidification process of multi-component alloys, where the liquidus temperature in solidification system can be obtained by:

$$T_{\text{liq}} = \overline{m_{\text{liq}}} \overline{C} + T_m \quad (11)$$

where

$$\overline{m_{\text{liq}}} = \frac{\sum_{i=1}^n (m_{\text{liq}}^i C^i)}{\overline{C}}, \quad \overline{C} = \sum_{i=1}^n C^i$$

In addition, the equilibrium partition coefficient of solutes in solidification system can be obtained from eq. (12). In this way, the updated equation of solid fraction in the solidification system of multi-component alloys are as eq. (13).

$$\overline{k_p} = \frac{\sum_{i=1}^n (k_p^i m_{\text{liq}}^i C^i)}{\sum_{i=1}^n (m_{\text{liq}}^i C^i)} \quad (12)$$

$$f_s = \frac{1}{1 - \overline{k_p}} \frac{T - T_{\text{liq}}}{T - T_m} \quad (13)$$

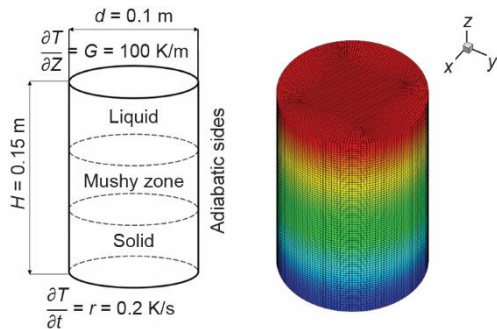


Figure 1. Schematic diagram of computational domain; (a) boundary condition and (b) grid used for simulation (for color image see journal web site)

Simulation conditions

The Ni-5.8 wt.% Al-15.2 wt.% Ta alloy always serves as a calculation example at the present simulation level. The computational domain, boundary conditions and grid used for simulation are shown in fig. 1, with the ingot height of 0.15 m and diameter of 0.1 m. In order to be closer to the production reality, the initial temperature field is set to be linearly distributed along the height direction with a temperature gradient G of 1000 K/m. The initial cooling temperature of bottom is 1685 K, and the cooling rate is 0.2 K/s.

It is assumed that the melt is instantly filled with whole casting, and the side wall is adiabatic. The boundary cooling condition of top is $\partial T/\partial z = G$, which is Neumann boundary condition. At the boundary, the solute field has no exchange with the outside and the velocity field is treated as no slip condition. The finite volume method has been adopted for simultaneously solving the coupled macroscopic mass, momentum, energy, and species conservation

equations. Based on the SIMPLEC algorithm, the commercial CFD software ANSYS FLU-ENT is employed to carry out simulations. Second-order discretization method for the convection terms is used to treat the fluid-flow in this paper. Besides, the simulation is performed using a computational time step of 0.01 seconds. Thermodynamic and transport properties used for calculation are shown in tab. 1 [18-20].

Table 1. Thermodynamic and transport properties of Ni-5.8 wt.% Al-15.2 wt.% Ta alloy

Parameters	Value	Parameters	Value
Density, ρ , [kgm^{-3}]	7365	Equilibrium partition coefficient, k^{Ta}	0.48
Specific heat, c_p , [$\text{Jkg}^{-1}\text{K}^{-1}$]	660	Solutal expansion coefficient, β_c^{Al} , [(wt.%) $^{-1}$]	2.26×10^{-2}
Thermal conductivity, λ , [$\text{Wm}^{-1}\text{K}^{-1}$]	80	Solutal expansion coefficient, β_c^{Ta} , [(wt.%) $^{-1}$]	-3.82×10^{-3}
Dynamic viscosity, μ , [$\text{kgm}^{-1}\text{s}^{-1}$]	4.9×10^{-3}	Reference concentration, $C_{l,ref}^{Al}$, [%]	5.8
Solutal diffusivity, D , [m^2s^{-1}]	5×10^{-9}	Reference concentration, $C_{l,ref}^{Ta}$, [%]	15.2
Latent heat, L , [Jkg^{-1}]	2.9×10^5	Reference temperature, T_{ref} , [K]	1685
Thermal expansion coefficient, β_r , [K^{-1}]	1.2×10^{-4}	Eutectic concentration, C_e^{Al} , [%]	37.5
Slope of liquidus, m^{Al} , [$\text{K}(\text{wt.}\%)^{-1}$]	-5.17	Eutectic concentration, C_e^{Ta} , [%]	76.1
Slope of liquidus, m^{Ta} , [$\text{K}(\text{wt.}\%)^{-1}$]	-2.55	Eutectic temperature, T_e , [K]	1560
Equilibrium partition coefficient, k^{Al}	0.54	Melting temperature, T_m , [K]	1754

Model verification

To verify the reliability of the previous developed multi-field coupled mathematical model, it was used to simulate a benchmark case of lateral solidification process of Sn-5 wt.% Pb alloy in a cavity that is 0.1 m long and 0.06 m wide. The parameters set in the simulation are consistent with those in the literature [21-23]. Based on this, the simulation results were compared with the results in the previous literatures. The cavity is only cooled on the left side, and the other boundaries are adiabatic, as is shown in fig. 2. The relative segregation ratio, S_{rel} , is defined to evaluate the local segregation degree inside the ingot:

$$S_{rel} = \frac{C - C_0}{C_0} 100\% \quad (14)$$

After solidification, the horizontal lines at the height of 25 mm and 55 mm inside the cavity were intercepted, and the relative segregation ratios on these lines obtained from the simulation were compared with the simulation and experimental data in the literatures, as shown in fig. 3. It can be found that the negative segregation is more obvious in the upper part

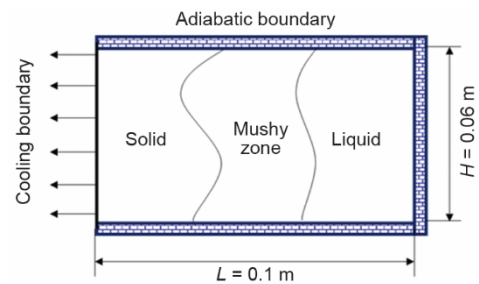


Figure 2. Schematic diagram of unidirectional solidification of Sn-5 wt.% Pb cooling from the side

of the cavity, while the middle and posterior of the lower part of the cavity show serious positive segregation along the solidification direction. The present predictions are generally consistent with the simulation results in the literature. In particular, the present predictions are more closer to the experimental data of Hebditch *et al.* [24] which is considered as a benchmark to verify the accuracy of their own models by later scholars. In summary, the reliability of mathematical model developed in this work is verified.

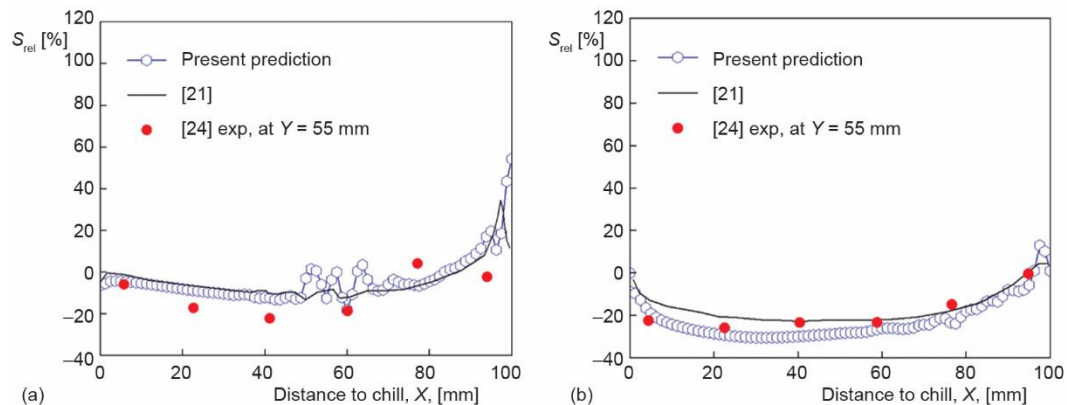


Figure 3. Comparison of relative segregation ratio S_{rel} at specific height from the bottom of the ingot at the end of solidification; (a) 25 mm and (b) 55 mm

Results and discussion

Flow field, solute and temperature distribution during solidification

In order to fully demonstrate the growth of solute enrichment channels and freckle formation inside the ingot, three moments during solidification were selected for research, which were 30%, 60% and 100% of the complete solidification time respectively. Figure 4 shows the enrichment channels of both solutes formed inside the ingot at 30% solidification ($t = 880$ seconds), and it can be found that the channel has begun to take shape at this moment. This is due to the fact that the equilibrium partition coefficients of both solutes are less than 1, and they are precipitated from the solid phase into the mushy zone. Therefore, density inversion is initially formed in the mushy zone, thus making the liquid therein unstable. In addition, the channels near the wall are significantly longer and richer in solute concentration. This is because the flow resistance at the ingot wall is much lower than that in the mushy zone, and thus the liquid convection is stronger and more conducive to the upward extension of the channels.

Since the solute conservation equation of Ta is the same as that of Al, the concentration distribution trends of both solutes are similar, which is also confirmed by fig. 4. Therefore, only the concentration distribution of solute Al will be shown and discussed below. In fig. 5(a), several channels are formed in both longitudinal sections ($X = 0, Y = 0$), around which there are all negative segregation of solute. It can be seen from fig. 5(b) that the locations of channels on cross section $X = 0$ are the final solidification region, and the liquid frac-

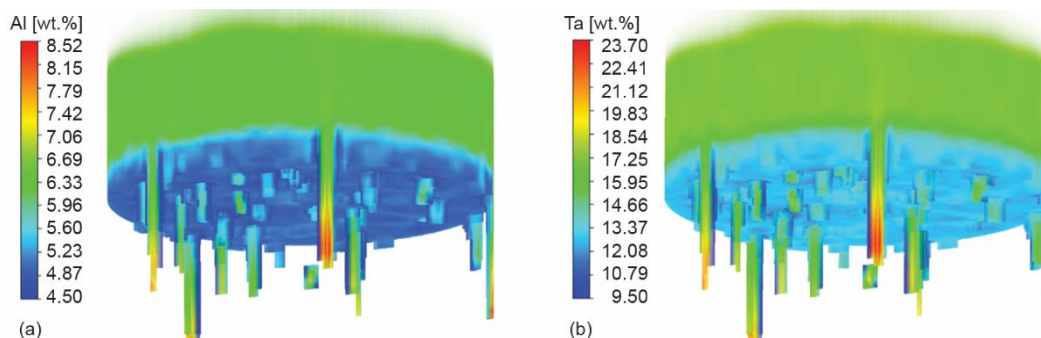


Figure 4. Enrichment channels of both solutes inside the ingot at 30% of full solidification time; (a) Al and (b) Ta (for color image see journal web site)

tion isosurface ($f_l = 0.9$) shows obvious crater-like fluctuations with upward jets at the location where the solute enrichment channels are formed. The solute-rich fluid continuously converges toward the channels of mushy zone, contributing to solute enrichment in these channels and solute shortage in the surrounding area during solidification. Density inversion caused by the combined effect of temperature and solute concentration gradients induces steady upward jets inside the channels, which also fundamentally explains why solute enrichment channels could appear and continue to grow. Two isosurfaces of liquid fraction are shown in fig. 5(c), which are used to approximate the liquidus and solidus line, respectively. There is a certain extent of fluctuation in the isotherms within the liquid region, mainly due to considerable disturbance caused by the flow pattern of multiple vortices, as shown in fig. 5(a).

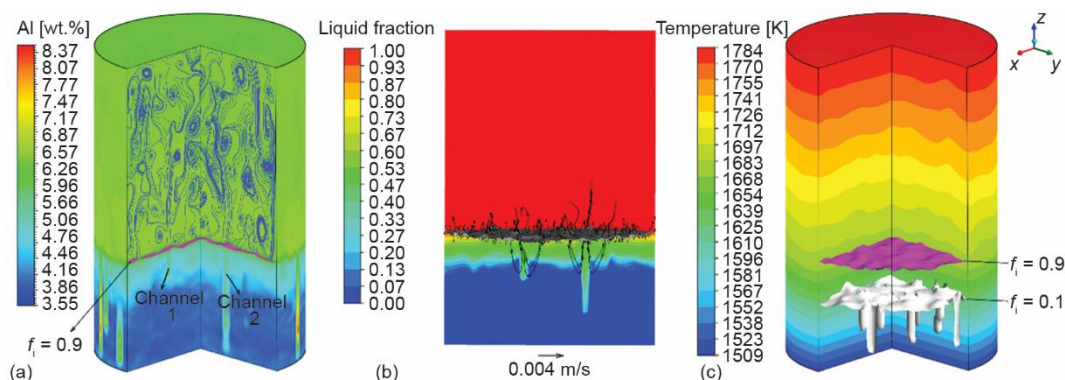


Figure 5. Results at 30% of full solidification time; (a) streamlines and solute distribution, (b) velocity field and liquid fraction at $X = 0$, and (c) temperature distribution (for color image see journal web site)

Figure 6 shows the channel segregation inside the ingot at the end of solidification ($t = 2900$ s). Combining figs. 6(a) and 6(b), it can be found that the solute enrichment areas show several channel-type distributions that correspond to the location of the freckles appearing at the top which are all positive segregation. As previously discussed, solute redistribution at the solidification front leads to solute accumulation in the solidification direction, and thus the final concentration of solute Al distributed at the top exceeds the initial value. The isotherms tend to be horizontal at the end of solidification, as shown in fig. 6(c). In order to more intuitively dis-

play the development of internal channels, two cross-sections of $Z = 0.05$ m and $Z = 0.1$ m in combination with the top are selected to observe the change of freckles after solidification as shown in fig. 6(d). Several freckles disappear from section $Z = 0.05$ m to $Z = 0.1$ m, indicating that channels at the corresponding location cannot keep growing all the time. There are multiple channels merging from $Z = 0.1$ m to the top, which will promote the growth of local solidification front and eventually form stable segregation channels. In theory, it can be explained by the fact that new solute accumulation around the channels may lead to new channels which compete to develop with each other. Induced by upward flow in the new channels, some original channels may deviate from its vertical development trend and even disappear due to the preferential growth of new channels. As a result, these original channels might merge with new channels or close directly without further development before reaching latter positions.

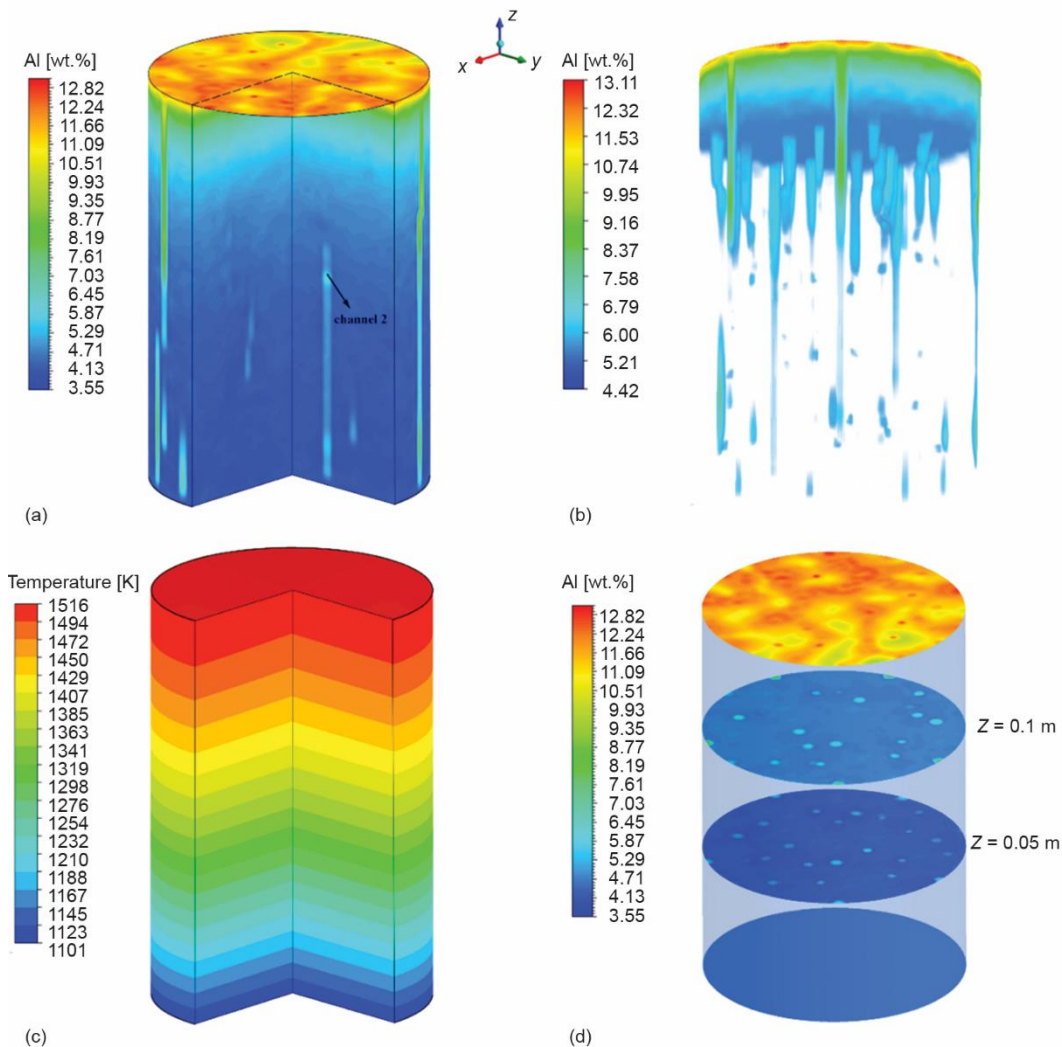


Figure 6. Results after solidification; (a) solute distribution, (b) solute enrichment channels of Al inside the ingot, (c) temperature distribution, and (d) development of segregation channels inside the ingot (for color image see journal web site)

Effect of cooling rate on freckle formation

As a crucial process parameter in actual production, cooling rate is closely related to the formation of freckles. Using several evaluation indexes, this work comprehensively analyzes and discusses its influence from qualitative and quantitative perspectives. Figure 7 shows the formation of freckles at the top under different cooling rates. It can be seen that with the increase of cooling rate, the number of freckles formed at the top gradually decreases, and so do the degree of solute enrichment at these freckles. One reason for this phenomenon is that the greater the cooling rate, the larger temperature difference between the bottom and the top of mushy zone. In this situation, density inversion in the mushy zone is more difficult to form, and then thermal-solute buoyancy is also harder to induce upward strong convection. Finally, solute enrichment channels will be more difficult to form. On the other hand, the greater cooling rate definitely leads to the faster solidification process and the lower permeability of mushy zone, then less liquid is supplied from the liquid region. Therefore, many channels are difficult to maintain steady growth so that the segregation degree of solutes will inevitably decrease.

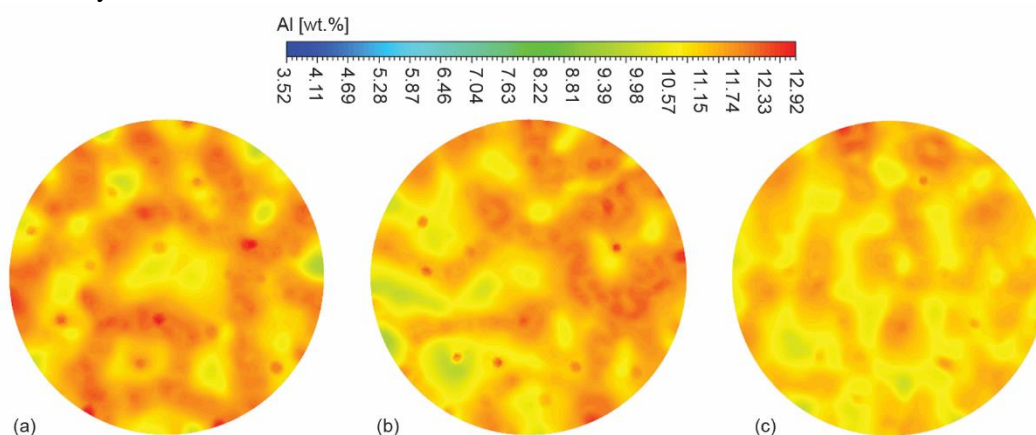


Figure 7. Freckle formation at the top of the ingot under different cooling rates; (a) 0.1 K/s, (b) 0.2 K/s, and (c) 0.5 K/s (for color image see journal web site)

The S_{rel} will convert to the minimum segregation ratio, S_{min} , and the maximum segregation ratio, S_{max} , when solute concentration is assigned its minimum and maximum values respectively. Besides, volume-averaged segregation ratio, S_{vol} , is defined to evaluate the overall segregation degree:

$$S_{vol} = \frac{\sum \sqrt{(C - C_0)^2} dV}{\sum dV} \frac{100\%}{C_0} \quad (15)$$

where C is the solute concentration on each grid centroid, C_0 – the initial solute concentration, and dV – the volume size of each grid.

The values of S_{min} obtained from fig. 8(a) decrease continuously with the increase of solidification time, which means negative segregation becomes more and more serious and reaches its peak after solidification. In the enlarged view, it can be found that the values of S_{min} gradually decrease with the increase of cooling rate at the initial stage of solidification. This is mainly due to the fact that thermosolutal convection and then solute segregation occur

earlier under a higher cooling rate at this moment. In this way, this fact can explain the phenomenon that the values of S_{\max} increase with growing cooling rate at the initial stage in fig. 8(b). However, it should be noticed that the pattern of segregation after solidification is the opposite. As the cooling rate changes from 0.1 K/s to 1.0 K/s, the final value of S_{\min} also increases from -43% to -41% . From fig. 8(b), it can be seen that the values of S_{\max} after solidification are generally identical under different cooling rates, remaining at about 173% . The most serious area of positive segregation is concentrated at the top of the ingot, while the intensity of thermosolutal convection near the top is fairly limited at the later stage of solidification. Therefore, the segregation degree is not greatly influenced by the change of cooling rate. As can be seen in fig. 8(c), the values of S_{vol} under different cooling rates always tend to increase first and then decrease, mainly due to the increasing negative segregation region as the solidification process proceeds. More importantly, it can be seen from figs. 8(a) and 8(b) that the absolute values of S_{\max} are larger than that of S_{\min} in general. As previously discussed, the values of S_{vol} will tend to decrease when there are enough negative segregation regions at the later solidification stage. In addition, the final value of S_{vol} decreases from 27% to 23% as the cooling rate increases from 0.1 K/s to 1.0 K/s, as shown in fig. 8(c).

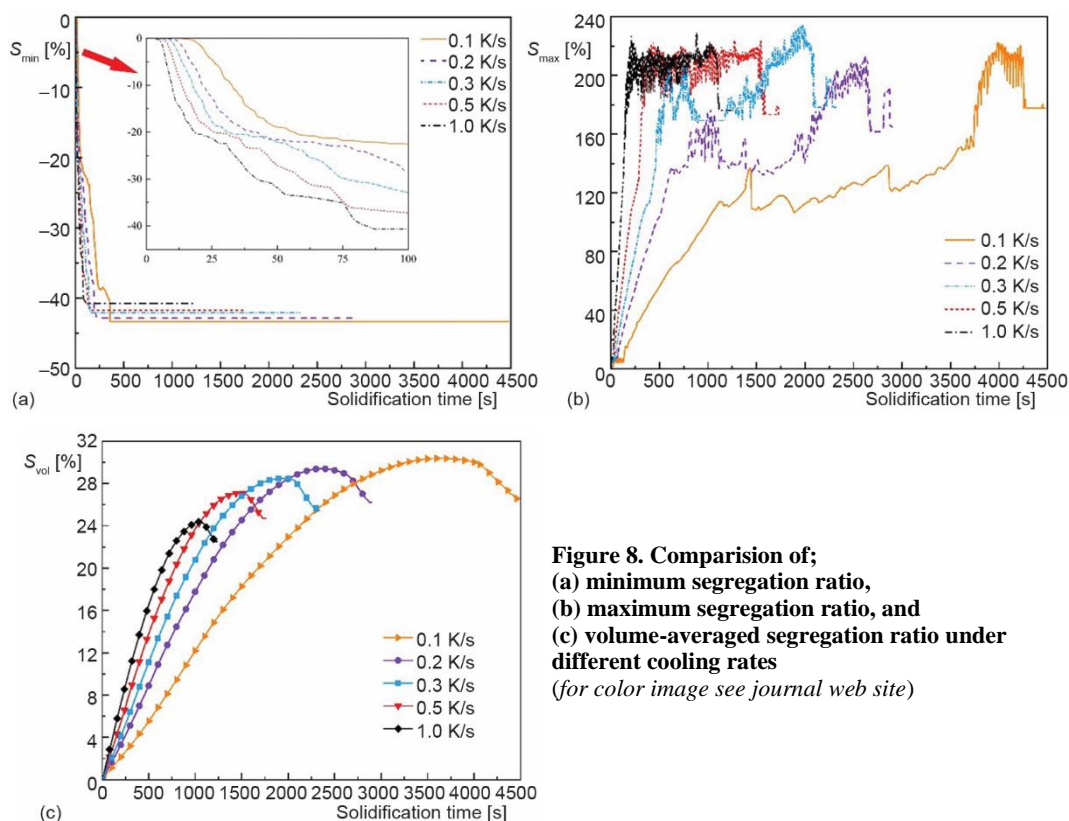


Figure 8. Comparison of;
(a) minimum segregation ratio,
(b) maximum segregation ratio, and
(c) volume-averaged segregation ratio under
different cooling rates
(for color image see journal web site)

In order to further explore the segregation degree inside the ingot after solidification, this study presents the volume size in each range of S_{rel} under different cooling rates from a local perspective, as shown in fig. 9. It should be noticed that the ranges of S_{rel} remain the same with the increase of cooling rate. Most of the areas inside the ingot are in the range of

–40% to 0, accounting for about 83% of the total volume. The span of S_{rel} for positive segregation inside the ingot is wider than that for negative segregation, but it accounts for less of the total volume. Due to the gradual accumulation of solutes during upward solidification, only the areas near the top and internal solute enrichment channels are positive segregation and the values of S_{rel} for negative segregation are more concentrated.

The numerical range of relative segregation ratio is divided into several parts as shown in tab. 2, which are defined as severe area (area 1), normal area (area 2), weak area (area 3) for positive segregation and weak area (area 4), normal area (area 5) for negative segregation. From tab. 2, it can be seen that the volume sizes of area 1, area 2, and area 3 do not show an obvious change pattern under different cooling rates, and these three areas account for a small proportion of the total volume. However, the volume sizes of area 4 and area 5 which account for a relatively large proportion increase and decrease respectively with growing cooling rate. Based on the comprehensive analysis, the proportion of weak area for segregation (–20%~20%) increases significantly from 26% at 0.1 K/s to 41% at 1.0 K/s, so that the segregation degree is weakened in general.

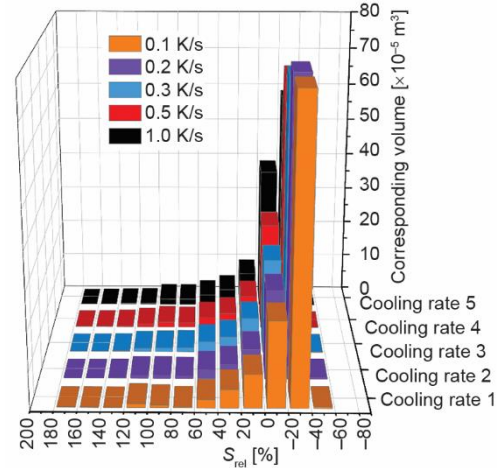


Figure 9. Volume size of each range of relative segregation ratio under different cooling rates
 (for color image see journal web site)

Table 2. Volume sizes and corresponding proportions of each defined area under different cooling rates

Cooling rate [Ks ⁻¹]	Volume sizes (× 10 ⁻⁵ m ³) and corresponding proportions				
	> 80%, area 1	20~80%, area 2	0~20%, area 3	–20%~0, area 4	< –20%, area 5
0.1	1.69 (1.43%)	7.21 (6.12%)	8.74 (7.42%)	22.31 (18.94%)	77.83 (66.08%)
0.2	1.81 (1.54%)	6.94 (5.89%)	7.88 (6.69%)	23.40 (19.87%)	77.74 (66.01%)
0.3	2.16 (1.83%)	8.19 (6.95%)	9.38 (7.96%)	25.23 (21.42%)	72.81 (61.82%)
0.5	2.60 (2.21%)	8.05 (6.84%)	8.93 (7.58%)	28.91 (24.55%)	69.27 (58.82%)
1.0	2.26 (1.92%)	8.89 (7.55%)	9.20 (7.81%)	38.66 (32.82%)	58.77 (49.9%)

Conclusions

In this work, a mathematical model for coupling flow field, solute distribution and temperature distribution during directional solidification of multi-component alloy is developed. After model verification, the dynamic growth of solute enrichment channels and the formation of freckles in Ni-5.8 wt.% Al-15.2 wt.% Ta alloy ingots are simulated. What's more, the effect of cooling rate on freckle formation and local segregation degree inside the ingot is analyzed and discussed. The main conclusions are as follows.

- The solute enrichment channels will grow continuously in the early stage of solidification, and then they keep developing and changing all the time during solidification. As multiple unstable channels merge or disappear directly, stable segregation channels are finally formed. After solidification, final channels formed in the ingot correspond to the

distribution of freckles at the top. The channels near the wall are more likely to keep growing, while most of the channels inside the ingot cannot continue to grow.

- With the increase of cooling rate, the number of freckles formed at the top gradually decreases, and so do the degree of solute enrichment at these freckles. As the cooling rate increases from 0.1 K/s to 1.0 K/s, the values of maximum segregation ratio after solidification are generally identical, remaining at about 173%. In this process, the final value of minimum segregation ratio increases from -43% to -41%, while the final value of volume-averaged segregation ratio decreases from 27% to 23%. In addition, the values of volume-averaged segregation ratio under different cooling rates always tend to increase first and then decrease.
- The span of relative segregation ratio for positive segregation inside the ingot is wider than that for negative segregation, but it accounts for less of the total volume. In contrast, the values of relative segregation ratio for negative segregation are more concentrated, and the numerical range of -40% to 0 can account for about 83% of the total volume. As the cooling rate increases from 0.1 K/s to 1.0 K/s, the proportion of weak segregation (-20% ~ 20%) increases significantly from 26% to 41%, so that the segregation degree is weakened in general.

Acknowledgement

This work was supported by the National Natural Science Foundation of China (Nos. 2017-VI-0015-0087, 2017-VI-0018-0090, 51690161) and Fundamental Research Funds for the Central Universities (No. N2125001). The authors are grateful for their financial support.

Nomenclature

C – average mass fraction of solutes, [wt.%]
 C_l – mass fraction of solutes in liquid phase, [wt.%]
 C_0 – initial mass fraction of solutes, [wt.%]
 C_s – mass fraction of solutes in solid phase, [wt.%]
 c_p – specific heat, [$\text{Jkg}^{-1}\text{K}^{-1}$]
 D – solutal diffusivity in the liquid, [m^2s^{-1}]
 f_l – liquid fraction
 f_s – solid fraction
 g – normal terrestrial gravity, [Nkg^{-1}]
 h – averaged specific enthalpy, [Jkg^{-1}]
 h_l – specific enthalpy in liquid phase, [Jkg^{-1}]
 h_s – specific enthalpy in solid phase, [Jkg^{-1}]
 K – mush permeability, [m^2]
 k_p – equilibrium partition coefficient
 L – latent heat, [Jkg^{-1}]
 m_{liq} – slope of liquidus, [$\text{K}(\text{wt.}\%)^{-1}$]
 p – pressure, [Pa]
 T – temperature, [K]
 T_{liq} – liquidus temperature, [K]
 T_m – pure solvent melting temperature, [K]

T_{sol} – solidus temperature, [K]
 t – time, [s]
 u – the fluid velocity in the x direction, [ms^{-1}]
 \vec{V} – velocity vector
 v – fluid velocity in the y direction, [ms^{-1}]
 w – fluid velocity in the z direction, [ms^{-1}]

Greek symbols

β_c – solutal expansion coefficient, [$(\text{wt.}\%)^{-1}$]
 β_T – thermal expansion coefficient, [K^{-1}]
 δ – secondary dendritic arm spacing, [m]
 λ – thermal conductivity, [$\text{Wm}^{-1}\text{K}^{-1}$]
 μ – dynamic viscosity, [$\text{kgm}^{-1}\text{s}^{-1}$]
 ρ – mass density, [kgm^{-3}]

Subscript

ref – reference values

Superscript

i – each component

References

- [1] Battaglioli, S., et al., Influence of Natural and forced Gravity Conditions During Directional Columnar Solidification, *International Journal of Heat and Mass Transfer*, 126 (2018), Nov., pp. 66-80
- [2] Kumar, A., et al., Channel Segregation During Columnar Solidification: Relation Between Mushy Zone Instability and Mush Permeability, *International Journal of Heat and Mass Transfer*, 164 (2021), Jan., 120602

- [3] Karagadde, S., et al., 3-D Microstructural Model of Freckle Formation Validated Using in Situ Experiments, *Acta Materialia*, 79 (2014), Oct., pp. 168-180
- [4] Zhang, B. J., et al., Recent Development of Nickel-Based Disc Alloys and Corresponding Cast-Wrought Processing Techniques, (In Chinese), *Acta Metallurgica Sinica*, 55 (2019), 9, pp. 1095-1114
- [5] Wang, L., et al., Gravitational Macro-segregation in Unidirectionally Solidified Lead-Tin Alloy, *Metallurgical Transactions A*, 19 (1988), Nov., pp. 2687-2694
- [6] Shevchenko, N., et al., Chimney Formation in Solidifying Ga-25wt pct In Alloys Under the Influence of Thermosolutal Melt Convection, *Metallurgical and Materials Transactions A*, 44 (2013), 8, pp. 3797-3808
- [7] Shevchenko, N., et al., Observation of Segregation Freckle Formation Under the Influence of Melt Convection, *IOP Conference Series: Materials Science and Engineering*, 27 (2012), 012085
- [8] Felicelli, S. D., et al., Modeling Freckle Formation in Three Dimensions During Solidification of Multi-component Alloys, *Metallurgical and Materials Transactions B*, 29 (1998), Aug., pp. 847-855
- [9] Bennon, W. D., Incropera, F. P., Numerical Analysis of Binary Solid-Liquid Phase Change Using a Continuum Model, *Numerical Heat Transfer*, 13 (1988), 3, pp. 277-296
- [10] Guo, J., Beckermann, C., Three-Dimensional Simulation of Freckle Formation during Binary Alloy Solidification: Effect of Mesh Spacing, *Numerical Heat Transfer, Part A: Applications*, 44 (2003), 6, pp. 559-576
- [11] Sung, P. K., et al., Sensitivity of Mesh Spacing on Simulating Macro-segregation During Directional Solidification of a Superalloy, *International Journal for Numerical Methods in Fluids*, 35 (2001), 3, pp. 357-370
- [12] Sun, Q. Y., et al., Numerical Investigations of Freckles in Directionally Solidified Nickel-Based Superalloy Casting with Abrupt Contraction in Cross Section, *Results in Physics*, 12 (2019), Mar., pp. 1547-1558
- [13] Kumar, A., et al., Effect of Discretization of Permeability Term and Mesh Size on Macro- and Meso-segregation Predictions, *Journal of Physics D: Applied Physics*, 42 (2009), 10, 105503
- [14] Rajeev, K., Das, S., A Numerical Study for Inward Solidification of a Liquid Contained in Cylindrical and Spherical Vessel, *Thermal Science*, 14 (2010), 2, pp. 365-372
- [15] Kaygisiz, Y., Maraşlı, N., Directional Solidification of Al-Cu-Si-Mg Quaternary Eutectic Alloy, *Journal of Alloys and Compounds*, 721 (2017), Oct., pp. 764-771
- [16] Wu, M., et al., Simulation of As-Cast Steel Ingots, *Steel Research International*, 89 (2018), 1, 1700037
- [17] Hetmaniok, E., et al., Solution of the Direct Alloy Solidification Problem Including the Phenomenon of Material Shrinkage, *Thermal Science*, 21 (2017), 1A, pp. 105-115
- [18] Tin, S., Pollock, T. M., Predicting Freckle Formation in Single Crystal Ni-Base Superalloys, *Journal of Materials Science*, 39 (2004), Dec., pp. 7199-7205
- [19] Kavooosi, V., et al., Influence of Cooling Rate on the Solidification Behavior and Microstructure of IN738LC Superalloy, *Journal of Alloys and Compounds*, 680 (2016), Sept., pp. 291-300
- [20] Sung, P. K., Poirier, D. R., Liquid-Solid Partition Ratios in Nickel-Base Alloys, *Metallurgical and Materials Transactions A*, 30 (1999), 8, pp. 2173-2181
- [21] Ahmad, N., et al., Numerical Simulation of Macro-segregation-a Comparison Between Finite Volume Method and finite Element Method Predictions and a Confrontation with Experiments, *Metallurgical and Materials Transactions A*, 29 (1998), Feb., pp. 617-630
- [22] Založnik, M., et al., An Operator Splitting Scheme for Coupling Macroscopic Transport and Grain Growth in a Two-Phase Multiscale Solidification Model: Part II – Application of the Model, *Computational Materials Science*, 48 (2010), 1, pp. 11-21
- [23] Li, W. S., et al., A Response to Numerical Benchmark for Solidification of Binary Alloys: Macro-Segregation with Thermosolutal Convection, *China Foundry*, 9 (2012), 2, pp. 171-177
- [24] Hebditch, D. J., Hunt, J. D., Observations of Ingot Macro-segregation on Model Systems, *Metallurgical and Materials Transactions B*, 5 (1974), 7, pp. 1557-1564